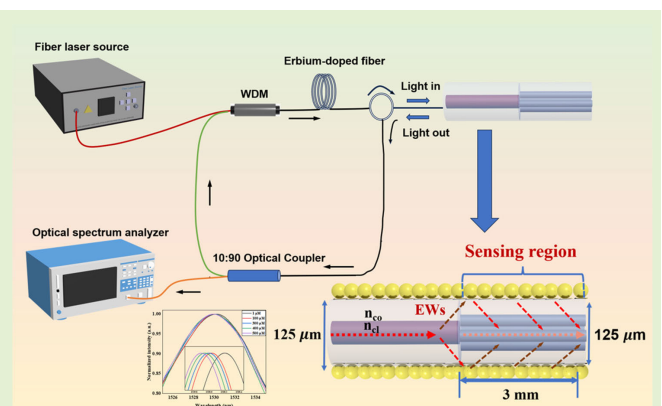


Laser-Based Four-Core Biosensor With WS₂ Thin-Film/CeO₂-Nanorods/AuNPs Immobilization for Ascorbic Acid Detection

Ziyi Liu, Xuecheng Liu, Ragini Singh^{ID}, Guoru Li, Sandip Swarnakar, Bingyuan Zhang^{ID}, and Santosh Kumar^{ID}, *Senior Member, IEEE*

Abstract—In this study, we present a novel optical sensing system for the real-time detection of ascorbic acid (AA), also known as vitamin C, a vital water-soluble vitamin with significant clinical relevance. AA serves not only as a biomarker for various diseases but also as a treatment for conditions such as scurvy, anemia, and cardiovascular disease. Our approach involves the development of a highly sensitive fiber optic sensor tailored for AA detection, utilizing a multimode fiber-four-core fiber (MMF-FCF) configuration. Fabrication involved advanced techniques, including fusion splicing and hydrofluoric (HF) acid etching, which created a core-mismatch structure generating sufficient evanescent waves (EWs). We immobilized tungsten disulfide (WS₂) thin-film and cerium dioxide nanorods (CeO₂-NRs) onto the probe's surface to enhance the sensor's performance. Thereafter, EWs excited the localized surface plasmon resonance (LSPR) phenomenon of gold nanoparticles (AuNPs) immobilized on the probe's surface, facilitating AA detection. To enhance AA sensor selectivity, the probe's surface was functionalized with the ascorbate oxidase (AOx) enzyme. The experiments utilized a laser source and an erbium-doped fiber amplifier (EDFA) to achieve precise excitation and signal amplification, enhancing the sensor's overall performance. Experimental results demonstrated a sensor sensitivity of 0.796 nm/mM and a limit of detection (LoD) of 167.71 μM within the 0–500 μM concentration range. These findings emphasize the sensor's potential value in clinical applications for AA detection.

Index Terms—Ascorbic acid (AA), Erbium-doped fiber amplifier (EDFA), fiber optic sensor, localized surface plasmon resonance (LSPR), multicore fiber.



I. INTRODUCTION

ASCORBIC acid (AA), known as an antioxidant, plays an active role in biological systems through different physiological functions, e.g., growth and repair of skin and

Manuscript received 7 September 2023; revised 6 October 2023; accepted 6 October 2023. Date of publication 16 October 2023; date of current version 14 November 2023. This work was supported in part by the Double-Hundred Talent Plan of Shandong, Liaocheng University, China, under Grant 318052341; in part by the Special Construction Project Fund for Shandong Taishan Mountain Scholars; in part by the Science and Technology Support Plan for Youth Innovation of Colleges and Universities of Shandong of China under Grant 2022KJ107; and in part by the Natural Science Foundation of Shandong under Grant ZR2020QC061 and Grant ZR2022QF137. The associate editor coordinating the review of this article and approving it for publication was Dr. Rui Min. (Corresponding authors: Ragini Singh; Bingyuan Zhang; Santosh Kumar.)

Please see the Acknowledgment section of this article for the author affiliations.

Digital Object Identifier 10.1109/JSEN.2023.3323392

connective tissue [1]. The occurrence of oxidative stress arises when the body's homeostasis is disrupted by the generation of free radicals that can contribute to the onset of various diseases, including posttraumatic tissue damage, chronic diseases, atherosclerosis, and cancer [2]. The utilization of AA can mitigate the risk of disease by effectively scavenging detrimental free radicals, thereby safeguarding other physiological functions from potential damage [3]. Adequate intake of amino acids can facilitate the synthesis of crucial amino acids necessary for collagen production. Conversely, a deficiency in AA can result in insufficient collagen levels within the body, leading to less elasticity in blood vessels and an increased susceptibility to scurvy [4]. Of course, the presence of collagen is also conducive to the protection of the skin, which has a role in delaying skin aging. Simultaneously, AA can inhibit the proliferation and metastasis of cancer cells, which plays a potential role in the treatment of

cancer [5], [6], [7]. AA has been significantly associated with serious diseases such as scurvy, Parkinson's disease, Alzheimer's disease, and cardiovascular disease in the human body [8]. Therefore, the health of the human body can be assessed by detecting the concentration of AA. AA has antioxidant properties, maintains a healthy balance in the body, and treats some specific diseases. However, the human body cannot synthesize AA by itself and can only supplement its content by ingesting it externally, which is also the case for most aquatic animals [9], and thus AA plays a great role for aquaculture as well. There are two primary methods for acquiring AA: through the consumption of fruits and vegetables and through the utilization of pharmaceuticals. In the 21st century, people are particularly concerned about their own health and the rejuvenation of their physical condition. The intake of AA should be maintained at 60–75 mg/day [9]. The AA detection content holds significant importance in assessing human health, as well as in the evaluation of medicinal and esthetic products. Therefore, there is a pressing need to create a sensitive, real-time, and convenient approach for the detection of AA content.

Presently, there are several established methodologies for the detection of AA, which encompass titration [10], [11], electrochemical detection [12], [13], and chromatography [14]. Nevertheless, a number of these methodologies exhibit some limitations, including exorbitant expenses, limited sensitivity, and intricate procedures. To overcome the constraints associated with the aforementioned methodologies, a novel laser-based fiber optic technology was employed that has gained significant traction in the field of biosensors. Fiber optics possess numerous advantageous attributes, including cost-effectiveness, robust resistance to interference, increased sensitivity, and other notable features. Various techniques, such as fiber core mismatch, tapered fiber, and etching, can be employed for the development of fiber optic biosensors. Among them, fiber core mismatch can provide the advantages of simplicity in operation, a high level of sensitivity, and compact size. In recent years, there has been an increasing proliferation of optical technology-based sensors, including but not limited to lossy mode resonance (LMR) [15], long-period grating (LPG) [16], and Mach-Zehnder interferometers (MZIs) [17]. Srivastava et al. [18] utilize a novel fiber optic structure to fabricate an effective sensor based on the in-fiber MZI. The device can enhance the sensitivity to the external refractive index (RI) through mode conversion phenomena. The localized surface plasmon resonance (LSPR) phenomenon has gained widespread attention because of developments in fiber optic technology and nanomaterials. Zhdanov [19] studied the sensors based on the principles of LSPR and surface plasmon resonance (SPR). A comprehensive elucidation of the functions performed by NPs, the process of sensor manufacturing, and the modeling techniques employed for LSPR and SPR sensors was provided, with the objective of elucidating the commonalities and distinctions between LSPR and SPR sensors. In the other hand, the high adsorption (e.g., cerium dioxide nanorods, CeO₂-NRs) and high surface area (e.g., WS₂) of nanomaterials allow for excellent biocompatibility. The ability to regulate the adhesion density

of nanomaterials on the surface of fibers is a significant advancement in enhancing the sensing capabilities of fiber optic probes [20].

The nature of LSPR sensors with coated nanoparticles depends strongly on the size, shape, and charge of the metal nanoparticles, which all affect the strength of the local electric field [21]. In this work, WS₂-thin layers, cerium dioxide CeO₂-NRs, and gold nanoparticles (AuNPs) were used to develop the proposed sensor probe. The WS₂ is an emerging material for constructing high-performance sensors with superior structural properties. WS₂ allows the possibility of changing the conductivity from metal to semiconductor, thus tuning the fluorescence and electrochemical properties [24]. Its unique lamellar 2-D structure can provide abundant attachment sites for AuNPs and AA to react with ascorbate oxidase (AOx). It has been shown that Au-WS₂ nanocomposites exhibit strong photoluminescence due to their LSPR effect [25]. Light absorption can be increased by the light trapping of WS₂, which can greatly limit the photoluminescence and detection rate through the enhancement of light-solid interaction [26]. The strong electric field strength of pure WS₂ nanosheets is a strong indication that WS₂ nanosheets have excellent LSPR effects [27]. Due to its high oxygen storage capacity and unique redox properties, the CeO₂ of the fluorite structure is widely used in gas sensing, water-gas shift reactions, and other fields [28]. CeO₂ is highly biocompatible and can maintain the activity of AOx coated on the probe, improve the survival rate of AOx, and enhance the sensitivity of the probe to the target substance. The small size of CeO₂-NRs has a very high surface effect and dielectric-limited domain effect, and the strong surface energy is favorable for the attachment rate of AOx and other nanomaterials.

In this work, the multimode fiber-four-core fiber (MMF-FCF) structure is used. Due to the structural properties of FCF itself, more light enters the cladding when light is injected from the MMF fiber into the FCF fiber. The mismatch between the FCF and the MMF is higher compared to the other structures. This study introduces a valuable approach for detecting AA, employing a fiber-core mismatch structure and leveraging the LSPR principle. This method overcomes the constraints associated with conventional detection techniques and offers a significant strategy for advancing AA sensor technology.

II. EXPERIMENTAL SECTION

A. Materials

The proposed structure was fabricated using traditional MMF (62.5/125 μm , Shenzhen Technologies Company Ltd., China) and FCF (8.0/125 μm , Fibercore Ltd., U.K.). AuNPs were synthesized with tetrachloroauric acid (HAuCl₄), trisodium citrate (Na₃C₆H₅O₇·2H₂O), and deionized (DI) water, and the probe surfaces were cleaned using acetone, hydrogen peroxide solution (H₂O₂, 30%), and concentrated sulfuric acid (H₂SO₄, 98%), and the AuNPs were immobilized with (3-mercaptopropyl) trimethoxysilane (MPTMS) and ethanol. The probes were immobilized with WS₂ thin-film, CeO₂-NRs. Then, 11-mercaptopundecanoic acid (MUA), N-hydroxysuccinimide (NHS), and N-(3-dimethylaminopropyl)-N-ethylenediimide hydrochloride (EDC) were utilized to

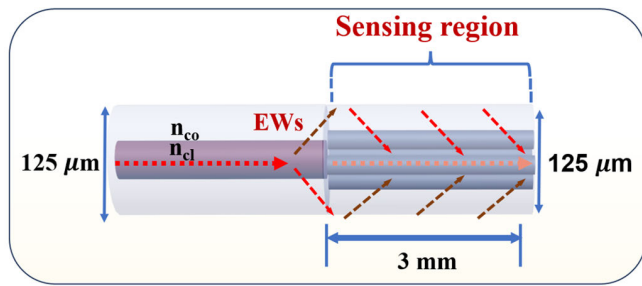


Fig. 1. Schematic of MMF-FCF-based fiber structure.

functionalize the AA enzyme. The nanomaterials of CeO₂ and WS₂ were purchased from Nanjing Xian Feng Nano Technology Company China. Phosphate-buffered saline (1 × PBS, pH = 7.4) was used to prepare various concentrations of AA solutions.

B. Instruments

The MMF-FCF probe structure was fabricated using a fusion splicer machine (FSM P100+, Fujikura), and the cross sections of the probes were scanned. A high-resolution transmission electron microscope (HR-TEM, Talos L120C, Thermo Fisher Scientific, USA) was used to observe the micro-distribution of the nanomaterials in the target solution. A UV-visible spectrophotometer (Hitachi-U-3310, Japan) was used to measure the absorption spectra of the AuNPs solution to determine the size of the AuNPs. The coating of nanomaterials on the probe surface was observed by scanning electron microscopy (SEM, Carl Zeiss Microscopy, Germany). Spectra were measured with an optical spectrum analyzer (OSA, AQ6370D, YOKOGAWA).

C. Sensing Mechanism of the Probe

To enhance the performance of the probe, it is necessary to intensify evanescent waves (EWs). The fiber was processed using fiber structure manufacturing techniques. Experiments employ a variety of technical procedures to fabricate fiber structures on a regular basis [22], [23], including changing the fiber structure (U-shaped), changing the fiber diameter (tapered fiber), reducing the cladding thickness (etching), and core-mismatch. This study employed two fiber production processes, namely core mismatch and etching, which are characterized by their cost-effectiveness and ease of fabrication. In this work, the MMF-FCF structure is adopted. Then, the fiber cladding is etched with hydrofluoric (HF) acid to generate more EWs, which lays an important foundation for the excitation of LSPR. The schematic of the sensor structure is shown in Fig. 1. The MMF and FCF were fused together using FSM to form a fiber mismatch structure. The optical spectra of various lengths of FCF were measured using an OSA that the optimal length of FCF is 3 mm. As a result, the entire probe area can be considered a new core, leading to the formation of a new optical waveguide with the external medium. This process generates a strong evanescent field, resulting in the probe exhibiting exceptional performance.

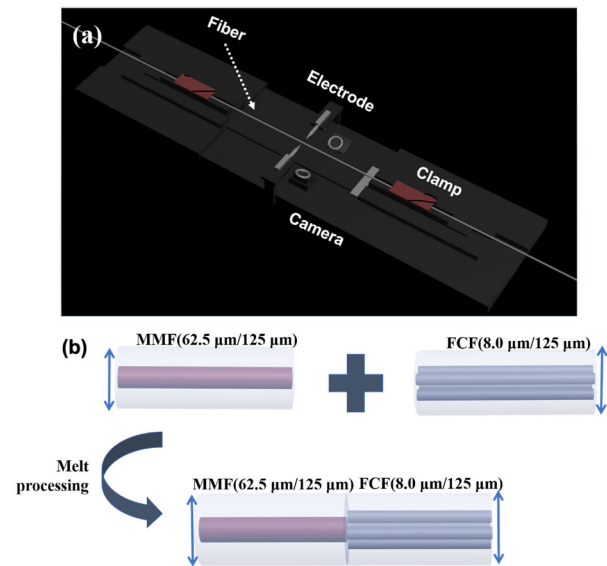


Fig. 2. (a) Internal structure of the FSM instrument. (b) MMF-FCF structure fabrication process.

D. Fabrication of Sensor Probe

This study utilized conventional MMF and FCF to construct the sensor probe. These two types of fibers were fused together using FSM to develop a core-mismatched structure. The process of fusion splicing was governed by a program. Several critical parameters played a significant role in this process, notably pre-discharge power, cleaning power, pre-melting power, and so on. The process of achieving loss-less fusion splicing with good repeatability of the fiber involves iterative debugging. This involves using the FSM with two electrodes that undergo continuous discharge to fuse the ends of the fiber. Additionally, the FSM produced a discharge field surrounding both sides of the fiber to ensure a more uniform discharge process. As a result, the FSM achieved a minimal loss of approximately 0 dB. The instrument structure of the FSM was operated with precision and a repeatable program to maximize the guarantee of repeatability in the discharge area. Fig. 2(a) and (b) show an internal view of the FSM machine and the proposed structure, respectively.

E. Synthesis Process of AuNPs-NPs/CeO₂-NRs/WS₂ Thin-Film

AuNPs with a particle size of 10 nm were synthesized by the Turkevich method [31]. First, HAuCl₄ was added to DI water and heated to boiling at 100 °C. At this time, the trisodium citrate solution was added. After 5 min, the color of the solution changed to that of red wine. Stirring was continued for 10 min to allow the solution to stabilize. CeO₂-NRs solution (3.125 mg/mL) was prepared with N-methylpyrrolidone and then sonicated for one hour. Similarly, WS₂ solution (1 mg/mL) was prepared with DI water and then sonicated for 2 h.

F. Nanocoating and Enzyme Functionalization

Nanomaterials are important for functionalizing probes and excitation of LSPR phenomena. Thus, immobilization and

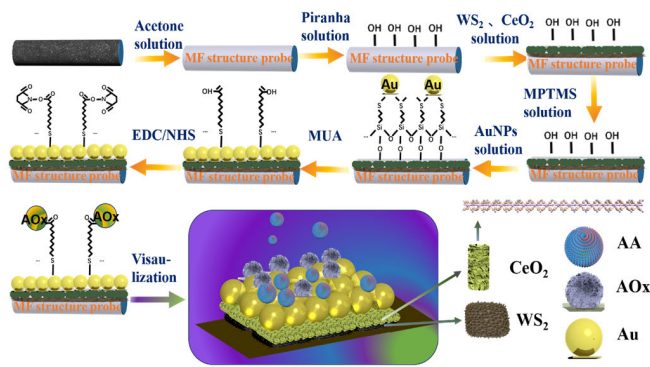


Fig. 3. WS_2 -thin layer/ CeO_2 -NRs/AuNPs-immobilization and AOX enzyme functionalization over MMF-FCF sensor structure.

functionalization of probes are critical in this work. The optical fiber was immersed in acetone for 20 min to remove organic contaminants from the surface of the fiber. And then the probe was immersed in Piranha solution (a mixture of sulfuric acid and 30% hydrogen peroxide, 7:3 by volume) for 30 min, which resulted in the formation of hydroxyl groups on the surface of the optical fiber to make it easier for immobilizing nanomaterials. After the above steps, the silanol groups on the surface of the MMF-FCF structured fiber were exposed, which helps the adhesion of MPTMS. Then, the optical fiber was immersed in the prepared WS_2 -thin layer solution for 10 min. The fiber was then dried in an oven at 70 °C for 30 min, and this step was repeated three times. A similar process was followed for the coating of CeO_2 -NRs.

The probe was then treated with a 1% MPTMS ethanol solution for 12 h. The methoxy group possessed by MPTMS can react with the silanol group to form a -SH group, which is beneficial for the immobilization of AuNPs. Then the probe was immersed in the synthesized AuNPs solution for 48 h. Au easily interacts with (-SH) to form stable Au-S covalent bonds, which immobilize AuNPs on the probe surface.

After the immobilization of nanomaterials, follow the enzyme functionalization process. The probe was first immersed in MUA ethanol solution (10 mL, 0.5 mM) for 5 h for carboxylation. Then the probe was immersed in 5 mL of a mixture of EDC (200 mM) and NHS (50 mM) for 30 min, which activated the carboxyl groups on the surface of the probe. The EDC and NHS converted the carboxyl groups into amino-active NHS esters. Finally, it was immersed in an aqueous solution of AOX for 12 h. The ester group of NHS reacted with AOX to achieve the functionalization of the enzyme. Fig. 3 shows the nanomaterial immobilization and enzyme functionalization processes.

G. Preparation of Analytes Solutions

In order to validate the sensing ability of the AOX sensor probe, five different concentrations of AA solutions at concentrations of 1, 100, 300, 400, and 500 μM were prepared for this work. The levels of AA in the human body are in the range of 40–120 μM ; thus, we prepared five solutions with different concentrations of AA to cover their highest and lowest concentrations. The pH within human blood is 7.35–7.45, and we prepared 1 \times PBS with 10 \times PBS to

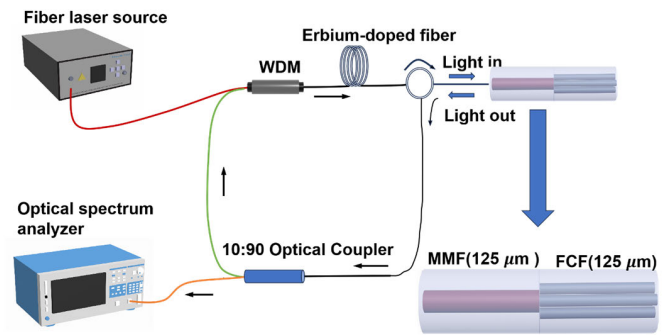


Fig. 4. Experimental setup for AA measurement.

provide an approximation of the pH of human blood, and a 2 mL stock solution was prepared by dissolving 35 mg of AA in 2 mL of 1 \times PBS solution. The remaining concentrations of AA solutions were then prepared by diluting the stock solution in 1 \times PBS.

H. Experimental Setup

The optical signal generated by the pump laser source (947 nm, Max-ray Photonics Company Ltd.) was received by the OSA, which accepted wavelengths in the range of 600–1700 nm. The schematic of the experimental setup is shown in Fig. 4. The experimental setup was constructed with a ring laser cavity, a 947 nm laser source to output the laser light, a 2 m long highly erbium-doped fiber (EDF) (ER12-6, Fibercore) with an absorption of 12 dB/m at 915 nm as the active medium, and a wavelength-division-multiplexer (WDM) coupler to feed the power into the cavity. The EDF used in the experiment improves the measurement accuracy and sensitivity of the sensor. An optical fiber consisting of MMF and FCF was inserted into the ring cavity together with a 10:90 coupler. Then, 10% of the coupler's output was used to transmit the laser output signal, which is monitored with an OSA, and 90% was fed into the cavity in the form of reflections, ensuring unidirectional operation so that this laser forms a ring cavity by reflection. When light passed through the sensing region, i.e., the region where the evanescent field was strong, the AuNPs absorbed the light and generated the resonance phenomenon. In addition, the light from the laser light source was transmitted through the optical fiber, and the specific enzyme on the probe couples with the target material, changing the RI surrounding the probe and altering the wavevector of the surface plasma wave, which causes a change in the EWs. The spectrum was measured using an OSA, which revealed that the peak of the resonance wave of the LSPR spectrum is shifted. Using this principle, the different levels of concentration of AA solution can be analyzed based on the LSPR spectrum of AA solution. The data corresponding to each concentration was recorded when the spectral output was stabilized.

III. RESULTS AND DISCUSSIONS

A. Optimization of Optical Fiber Sensor Probe

This section elucidates the methodology employed for ascertaining the splicing parameters and optimizing the etching time of the fiber optic sensor. The crucial stage in the fusion splicing of optical fibers using an FSM is to appropriately calibrate the fusion procedure parameters.

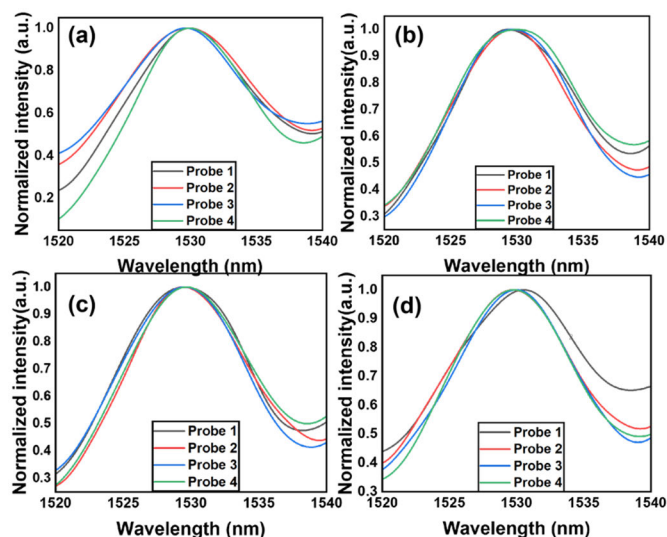


Fig. 5. Repeatability analysis of MMF-FCF sensor structures with FCF lengths of (a) 1 mm, (b) 2 mm, (c) 3 mm, and (d) 4 mm.

The determination of the ideal experimental parameters involved iterative experimentation, wherein the experimental debugging process was repeated and adjustments were made to the parameters. This approach aimed to generate a fiber probe that exhibited high sensitivity and excellent repeatability.

The MMF-FCF structure was influenced by the length of the FCF, and it was necessary to fabricate this structure using FCF lengths of 1–4 mm. The transmitted intensities of the fiber optic probes with these different FCF lengths were then measured. The resulting transmitted intensities were depicted in Fig. 5(a)–(d) for the fiber optic probes with FCF lengths of 1–4 mm, respectively. The transmitted spectra of the fiber probes were measured for four kinds of fiber probes. Fig. 5(c) illustrates that the fiber with a FCF of 3 mm exhibited the highest level of repeatability. In theory, a decrease in transmitted intensity corresponds to an increase in the amount of light injected into the core, whether it is located inside or outside the cladding. This increase in light injection leads to the generation of additional EWs, which in turn enhances the stimulation of the LSPR phenomenon. From Fig. 6(a), comparing the transmitted intensities of different MMF-FCF structures, it can be concluded that the FCF length of 3 mm was the lowest transmitted intensity, thus the MMF-FCF structure with an FCF length of 3 mm was selected to develop the sensor probe.

The relationship between etching time and cladding layer thickness was evident, with longer etching times resulting in a smaller cladding layer thickness.

However, this did not necessarily imply that a smaller cladding layer thickness was superior. By examining the transmitted intensity spectra of the MMF-FCF structure at different etching times [as shown in Fig. 6(b)], it was observed that the fiber optic probe etched for 10 min exhibited the lowest transmitted intensity. Similarly, the fiber optic fiber yielded the lowest transmitted intensity. The light probe exhibited the lowest transmitted intensity, resulting in the generation of highly potent EWs under this particular parameter. Hence, the fiber optic probe with an etching time of 10 min and an FCF length

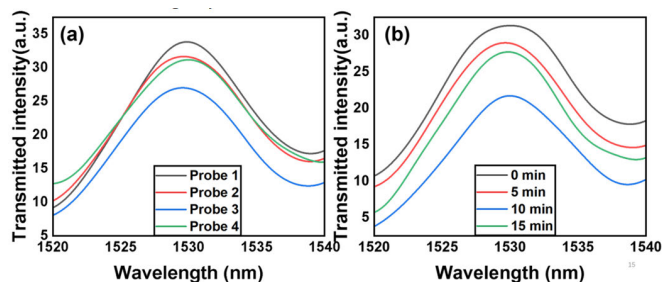


Fig. 6. (a) Comparison of the transmitted intensity of different MMF-FCF structures (probe 1 –1 mm, probe 2 –2 mm, probe 3 –3 mm, probe 4 –4 mm). (b) Transmitted intensity spectra of MMF-FCF structures at different etching times.

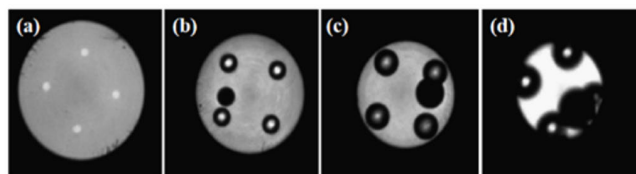


Fig. 7. MMF-FCF structure at different etching times (a) 0 min, (b) 5 min, (c) 10 min, and (d) 15 min.

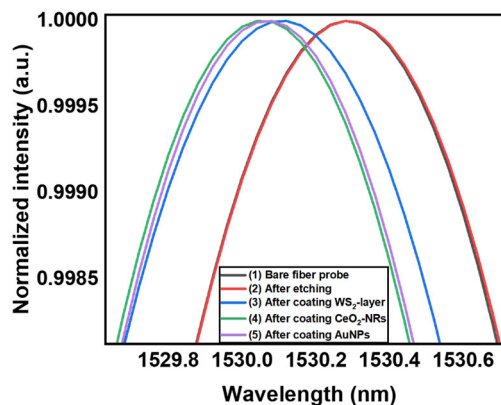


Fig. 8. Transmission intensity spectra at different treatment stages (bare fiber, etched, coated with WS₂-thin film, CeO₂-NRs, and AuNPs, respectively).

of 3 mm was chosen. Once the fabrication of the optical fiber was completed and the optimal length of the FCF was identified, the fiber underwent a series of etching processes using HF acid at various durations. The objective was to ascertain the most suitable etching time for achieving optimal results. Fig. 7 illustrates the cross-sectional configuration of the MMF-FCF, showcasing changes resulting from varying etching durations. The fiber probes underwent etching processes lasting 0, 5, 10, and 15 min, with corresponding cross-sectional perspectives presented in Fig. 7(a)–(d), respectively. These images reveal the expansion of the core diameter and the reduction in the external cladding diameter as the etching time progresses.

The transmitted intensity spectra at different processing stages, such as: 1) bare fiber probe; 2) after etching; 3) after coating of WS₂-thin layer; 4) after coating of CeO₂-NRs; and 5) after coating of AuNPs, are shown in Fig. 8, and it can be observed that, the spectral peaks of the fiber are affected at different processing steps.

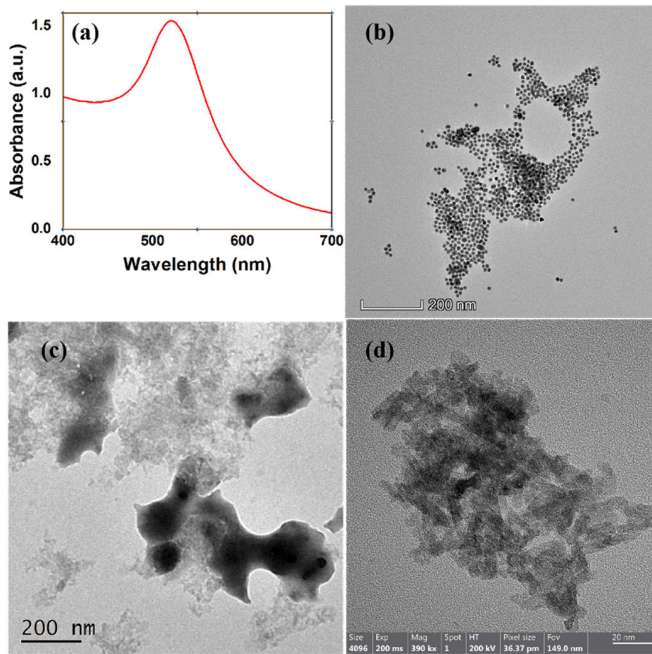


Fig. 9. (a) Absorbance spectrum of AuNPs. (b) TEM image of AuNPs. (c) TEM image of WS_2 thin-film. (d) TEM image of CeO_2 -NRs.

B. Characterization of Nanomaterials

The sensing performance can be significantly influenced by the size and shape of the AuNPs, with the LSPR effect exhibiting an exponential decrease as the nanoparticle morphology and scale varied from 10 to 50 nm [32].

The absorption spectrum of the synthesized AuNPs solution was measured using a UV-visible spectrophotometer. The results are shown in Fig. 9(a), and the absorption peak of the AuNPs solution was at 520 nm, which indicated that the size of the AuNPs in our synthesized solution was around 10 nm. Thus, the morphology of AuNPs was observed by HR-TEM, and the results are shown in Fig. 9(b). It can be seen that the synthesized AuNPs are spherical and uniform in size, which makes them easy to resonate with the EWs and excite the LSPR phenomenon. As shown in Fig. 9(c) and (d), a large amount of WS_2 thin-film and CeO_2 -NRs are observed in the synthesized solution, which increased the probability of attachment of the AOX enzyme to the probe.

C. Characterization of NPs-Immobilized Structure

The immobilization of nanomaterials was crucial for the experiment. The fabricated probe was scanned with SEM, and the result was used to verify whether the nanomaterials were well-mobilized on the MMF-FCF probes.

The SEM result showed that the WS_2 , CeO_2 -NRs, and AuNPs were efficiently immobilized on the surface of the probe, as shown in Fig. 10. The prepared WS_2 -thin film layer is flat-structured nanosheets, according to Fig. 9. It can be seen in Fig. 10 that the flat nanosheets are uniformly immobilized on the fiber surface. Furthermore, CeO_2 -NRs were also coated uniformly according to the experimental result. Whereas, AuNPs exhibited a consistent morphology, characterized by a spherical form with a diameter of around 10 nm.

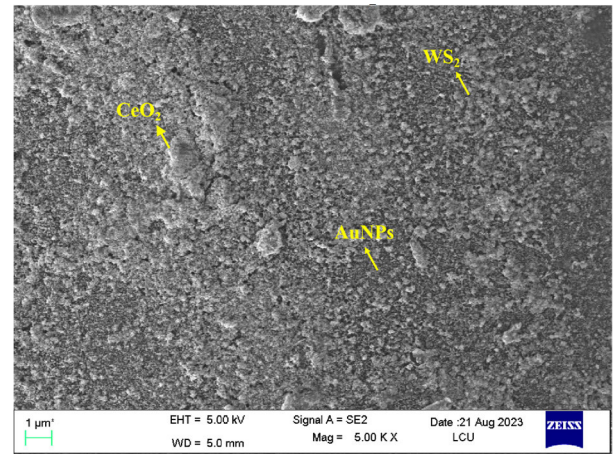


Fig. 10. SEM image of WS_2 thin-film, CeO_2 -NRs, and AuNPs-immobilized MMF-MCF probe.

The illustration shown in Fig. 10 clearly illustrates the uniform coating of AuNPs.

D. Measurement of AA Solutions

Different AA solutions with concentrations ranging from 1 μM to 500 mM were detected using the developed sensor probes. This range covered the lowest and highest AA concentrations in the human body. Before detecting the first concentration of AA solution, the probes were rinsed with PBS solution. After the sensor probe was dried, the respective transmitted intensity and wavelength were recorded, guaranteeing the initial pH of the probe. Then, the probe was rinsed with $1 \times \text{PBS}$ and dried at room temperature, after which other concentrations of AA solutions were measured. Before measuring the next sample, the sensor probe must be cleaned with a PBS solution to minimize the crosstalk error between the new AA concentration and residual molecules on the fiber surface. According to the above steps, LSPR spectra were recorded for all concentrations, and the obtained results were expressed as transmitted intensity spectra. First, a 1 μM concentration of AA solution was added to the sensor probe, and the respective LSPR spectra were recorded.

All solutions were tested three times with three different probes. For our developed probes, LSPR spectra are shown in Fig. 11(a). According to the results, it can be implied that the LSPR spectral peak decreased with increasing concentration. It can be seen in Fig. 11(b) that the linear relationship between the peak wavelength of the LSPR spectra and the AA solutions was expressed as

$$\lambda = 0.000796 C + 1529.96. \quad (1)$$

In (1), λ is the peak wavelength, C is the concentration of AA solution, and the slope is the sensitivity of the probe. By measuring the $1 \times \text{PBS}$ solution fifteen times with the same probe, the data were recorded each time after the LSPR spectra were stabilized. The standard deviation (SD) was calculated from the resonance peak wavelengths of the fifteen times $1 \times \text{PBS}$ data.

The limit of detection (LoD) serves as a pivotal measure of the biosensor's stability and sensitivity. LoD represents the

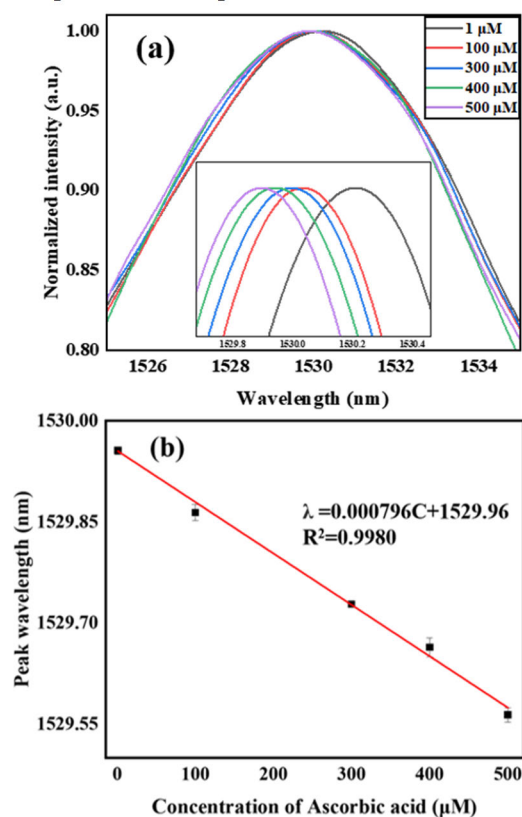


Fig. 11. Measurement of AA using the proposed MMF-FCF-based fiber structure. (a) Sensing spectrum. (b) Linear plot of the proposed sensor.

minimum concentration at which the biosensor can effectively detect analytes. It was determined by performing an inverse fit function on the fit curve. And it can be calculated using the following formula [33]:

$$\text{LoD} = \frac{3 \times \text{SD}}{\text{Sensitivity}}. \quad (2)$$

According to the calculation, the LoD of the developed AA sensor is 167.71 μM .

E. Stability Test and Selectivity Test

The stability test is performed to investigate whether the peak wavelength position of the sensor probe is stable over multiple measurements. Excellent stability of the probe is required to ensure the accuracy of the measurement results when the probe is applied. Initially, the probe was submerged in a PBS solution.

Subsequently, the probe's spectra were assessed and documented. Following the drying of the probe's surface, the PBS solution was reintroduced. The PBS solution was tested with the same probe 15 consecutive times. The results were then analyzed according to the resonance wavelength of the peak. The test results of stability are shown in Fig. 12(a), which shows that the developed probe has almost the same resonance wavelength in 15 measurements with an SD of 0.0445, indicating that the probe possesses good stability.

Selectivity is the most important characteristic of a sensor. The purpose of the selectivity test is to detect whether the sensor has the ability to resist the influence of other external

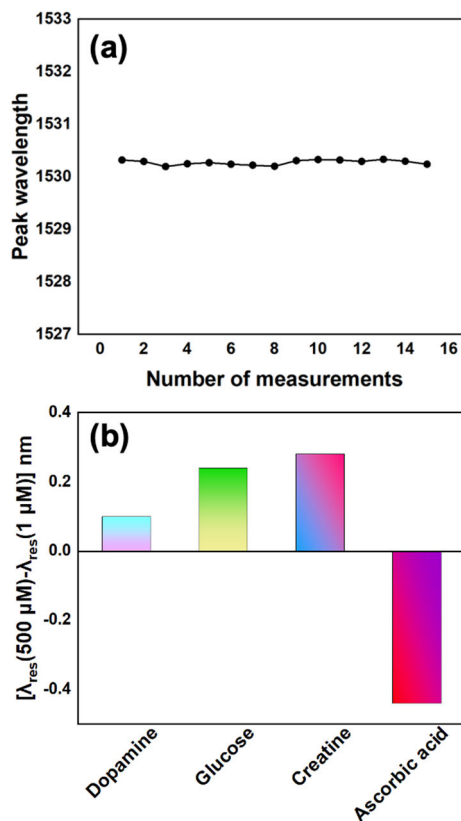


Fig. 12. (a) Stability test of the developed sensor. (b) Selectivity result.

interfering substances. For this reason, three other substances were arbitrarily chosen to measure their LSPR spectra, namely dopamine, glucose, and creatine. The LSPR spectra of the three other substances were measured at concentrations of 1–500 μM , respectively, and the results of the test are shown in Fig. 12(b). The resonance peak of the LSPR spectra observed the most significant change as a result of variation in the concentration of the AA solution. Consequently, the probe that developed exhibits good selectivity.

F. Reproducibility and Reusability Test

The reproducibility of the probes was examined by measuring the same concentration of AA solution with different sensor probes. In this experiment, three identical probes were used to detect AA solutions at a concentration of 400 μM . The LSPR spectra were allowed to stabilize, and the data were recorded. As shown in Fig. 13(a), for the same concentration of AA solution, the resonance wavelengths of the different probes were basically similar, indicating that the probe has good reproducibility.

Reusability is another important attribute of high-performance probes. If the probe can be reused and performs well, it indicates that the developed probe is practical in the application and can eliminate the errors caused by different probes measuring the same substance. The same sensor probe was used to measure two concentrations of AA solution twice. First, the probe was immersed in a 100 μM concentration of AA solution, and its data were recorded after the LSPR spectrum was stabilized. Then, the probe was immersed

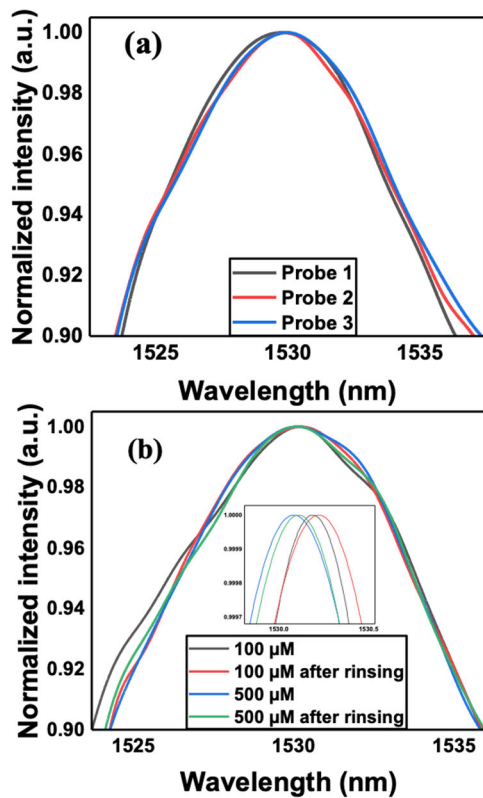


Fig. 13. (a) Reproducibility test. (b) Reusability of the developed sensor.

TABLE I
PERFORMANCE COMPARISON OF THE PROPOSED
SENSOR WITH THE EXISTING AA SENSORS

Nano-materials used	Mechanisms	Linear range	Sensitivity	LoD	Ref.
CoOOH NPs	Fluorescence	0.5 μM –20 μM	n.r. ^a	0.47 μM	[34]
AuNPs	Chemical analysis	10.6–70.4 μM	134 $\mu\text{Ac}m^{-2}/\text{mgL}^{-1}$	n.r. ^a	[35]
MWCNTs	Chemical analysis	5–110 μM	n.r. ^a	9.9 nM	[36]
AuNPs	Plasmon resonance absorption	2.5–17.5 μM	6.592 nm/mM	0.48 μM	[37]
AuNPs	Rapid colorimetric determination	1.0–9.0 mg dm^{-3}	n.r. ^a	0.8 mg dm^{-3}	[38]
CuONPs	Chemical analysis	10–150 μM	0.103 V $\log(\mu\text{M})^{-1}$	1.97 μM	[39]
AuNPs	LSPR	1–500 μM	0.796 nm/mM	167.71 μM	This work

^anot reported

in $1 \times \text{PBS}$ solution, gently stirred, and taken out to dry naturally, and the 100 μM concentration of AA solution was measured again. Similarly, a 500 μM AA solution was measured, and the results are shown in Fig. 13(b). It can be seen that the probes have basically similar peak wavelengths at the same concentration, which indicates that the developed sensor probes have good reusability.

G. Evaluation of Sensing Performance

Currently, many methods for AA detection include electrochemical, titration, fluorescence, and so on. Table I shows the comparison of the sensing performance of the developed AA sensor with other methods to measure AA. The most widely used technique for the determination of AA is titration. However, titration has low sensitivity. In this work, an AA sensor based on the simple, portable, and sensitive biosensor structure of MMF-FCF is proposed. The advantages of this method included low cost, wide detection range, high sensitivity, real-time performance, ease of operation, and high feasibility.

IV. CONCLUSION

In this study, the authors have developed a laser-based fiber-optic sensing probe using a unique MMF-FCF structure to detect different concentrations of AA by using the LSPR phenomenon induced by AuNPs. The probe's evanescent field is amplified through the fiber core mismatch structure and selective etching to activate the LSPR phenomenon.

WS_2 thin-film and CeO_2 -NRs are applied to the probes to enhance the surface area for AuNPs and AOx attachment while preserving enzyme activity. These tailored probes are immersed in solutions with different AA concentrations, and the LSPR spectra are recorded. The AA concentration is determined by monitoring the shift in the resonance peak wavelength. The results demonstrated a linear correlation between the AA solution and the wavelength shift within the concentration range of 1–500 μM , with a remarkable linear fit value of 0.9980. Overall, this innovative fiber-optic sensing probe, capitalizing on the MMF-FCF structure and LSPR phenomenon, exhibits substantial potential for precise AA detection. Its further development could significantly advance analytical capabilities and applications in diverse fields.

ACKNOWLEDGMENT

Ziyi Liu is with the Ji Xianlin College and the School of Physics Science and Information Technology, Liaocheng University, Liaocheng 252059, China (e-mail: 1003771607@qq.com).

Xuecheng Liu, Guoru Li, and Bingyuan Zhang are with the Shandong Key Laboratory of Optical Communication Science and Technology, School of Physics Science and Information Technology, Liaocheng University, Liaocheng 252059, China (e-mail: xue_chengliu@163.com; grli@lcu.edu.cn; zhangbingyuan@lcu.edu.cn).

Ragini Singh is with the College of Agronomy, Liaocheng University, Liaocheng 252059, China (e-mail: singh@lcu.edu.cn).

Sandip Swarnakar is with the Department of ECE, K. L. Deemed to be University, Guntur, Andhra Pradesh 522302, India (e-mail: sandipswarnakar.2008@gmail.com).

Santosh Kumar is with the Shandong Key Laboratory of Optical Communication Science and Technology, School of Physics Science and Information Technology, Liaocheng University, Liaocheng 252059, China, and also with the Department of ECE, K. L. Deemed to be University, Guntur, Andhra Pradesh 522302, India (e-mail: santosh@lcu.edu.cn).

REFERENCES

- B. Özkahraman, G. Torkay, Z. Özbaş, and A. Bal-Öztürk, "The effect of vitamin C in the formulation of pectin/thiolated alginate buccal adhesive patches: In vitro and ex vivo evaluation," *Int. J. Adhes. Adhesives*, vol. 120, Jan. 2023, Art. no. 103276, doi: 10.1016/j.ijadhadh.2022.103276.
- J. Reang, P. C. Sharma, V. K. Thakur, and J. Majeed, "Understanding the therapeutic potential of ascorbic acid in the battle to overcome cancer," *Biomolecules*, vol. 11, no. 8, p. 1130, Jul. 2021, doi: 10.3390/biom11081130.

- [3] J. Baek, M. Ramasamy, N. C. Willis, D. S. Kim, W. A. Anderson, and K. C. Tam, "Encapsulation and controlled release of vitamin C in modified cellulose nanocrystal/chitosan nanocapsules," *Current Res. Food Sci.*, vol. 4, pp. 215–223, Jan. 2021, doi: [10.1016/j.crfs.2021.03.010](https://doi.org/10.1016/j.crfs.2021.03.010).
- [4] P. Duque, C. P. Vieira, B. Bastos, and J. Vieira, "The evolution of vitamin C biosynthesis and transport in animals," *BMC Ecol. Evol.*, vol. 22, no. 1, p. 84, Dec. 2022, doi: [10.1186/s12862-022-02040-7](https://doi.org/10.1186/s12862-022-02040-7).
- [5] E. Pawlowska, J. Szczepanska, and J. Blasiak, "Pro- and antioxidant effects of vitamin C in cancer in correspondence to its dietary and pharmacological concentrations," *Oxidative Med. Cellular Longevity*, vol. 2019, Dec. 2019, Art. no. 7286737, doi: [10.1155/2019/7286737](https://doi.org/10.1155/2019/7286737).
- [6] M. Attia, E. A. Essa, R. M. Zaki, and A. A. Elkordy, "An overview of the antioxidant effects of ascorbic acid and alpha lipoic acid (in liposomal forms) as adjuvant in cancer treatment," *Antioxidants*, vol. 9, no. 5, p. 359, Apr. 2020, doi: [10.3390/antiox9050359](https://doi.org/10.3390/antiox9050359).
- [7] T.-M. Wu, S.-T. Liu, S.-Y. Chen, G.-S. Chen, C.-C. Wu, and S.-M. Huang, "Mechanisms and applications of the anti-cancer effect of pharmacological ascorbic acid in cervical cancer cells," *Frontiers Oncol.*, vol. 10, pp. 1–12, Sep. 2020, doi: [10.3389/fonc.2020.01483](https://doi.org/10.3389/fonc.2020.01483).
- [8] G. J. Kontoghiorghes, A. Kolnagou, C. N. Kontoghiorghes, L. Mourouzidis, V. A. Timoshnikov, and N. E. Polyakov, "Trying to solve the puzzle of the interaction of ascorbic acid and iron: Redox, chelation and therapeutic implications," *Medicines*, vol. 7, no. 8, p. 45, Jul. 2020, doi: [10.3390/medicines7080045](https://doi.org/10.3390/medicines7080045).
- [9] X. Yin et al., "Chemical stability of ascorbic acid integrated into commercial products: A review on bioactivity and delivery technology," *Antioxidants*, vol. 11, no. 1, p. 153, Jan. 2022, doi: [10.3390/antiox11010153](https://doi.org/10.3390/antiox11010153).
- [10] N. Kaewchuay, J. Jantra, C. Khetlatat, S. Ketnok, N. Peungpra, and S. Teeppo, "On-site microfluidic paper-based titration device for rapid semi-quantitative vitamin C content in beverages," *Microchem. J.*, vol. 164, May 2021, Art. no. 106054, doi: [10.1016/j.microc.2021.106054](https://doi.org/10.1016/j.microc.2021.106054).
- [11] O. Heidary, M. Akhond, and B. Hemmateenejad, "A microfluidic paper-based analytical device for iodometric titration of ascorbic acid and dopamine," *Microchem. J.*, vol. 182, Nov. 2022, Art. no. 107886, doi: [10.1016/j.microc.2022.107886](https://doi.org/10.1016/j.microc.2022.107886).
- [12] P. Deng et al., "Application of a simple and sensitive electrochemical sensor in simultaneous determination of paracetamol and ascorbic acid," *J. Electrochem. Soc.*, vol. 168, no. 9, Sep. 2021, Art. no. 096501, doi: [10.1149/1945-7111/ac1e59](https://doi.org/10.1149/1945-7111/ac1e59).
- [13] Y. Wu et al., "Simultaneous and sensitive determination of ascorbic acid, dopamine and uric acid via an electrochemical sensor based on PVP-graphene composite," *J. Nanobiotechnol.*, vol. 18, no. 1, p. 112, Aug. 2020, doi: [10.1186/s12951-020-00672-9](https://doi.org/10.1186/s12951-020-00672-9).
- [14] Y. Xing et al., "Vitamin C supplementation is necessary for patients with coronavirus disease: An ultra-high-performance liquid chromatography-tandem mass spectrometry finding," *J. Pharmaceutical Biomed. Anal.*, vol. 196, Mar. 2021, Art. no. 113927, doi: [10.1016/j.jpba.2021.113927](https://doi.org/10.1016/j.jpba.2021.113927).
- [15] S. Choudhary, F. Esposito, L. Sansone, M. Giordano, S. Campopiano, and A. Iadicicco, "Lossy mode resonance sensors in uncoated optical fiber," *IEEE Sensors J.*, vol. 23, no. 14, pp. 15607–15613, Jul. 2023, doi: [10.1109/JSEN.2023.3280675](https://doi.org/10.1109/JSEN.2023.3280675).
- [16] F. Esposito, "(INVITED)Chemical sensors based on long period fiber gratings: A review," *Results Opt.*, vol. 5, Dec. 2021, Art. no. 100196, doi: [10.1016/j.rio.2021.100196](https://doi.org/10.1016/j.rio.2021.100196).
- [17] T. Wang, B. Liu, L. Zhao, Y. Mao, J. Ren, and J. Zheng, "High-sensitivity liquid level sensor based on the balloon-shaped fiber optic MZI," *IEEE Photon. J.*, vol. 14, no. 2, pp. 1–7, Apr. 2022, doi: [10.1109/JPHOT.2022.3160735](https://doi.org/10.1109/JPHOT.2022.3160735).
- [18] A. Srivastava, F. Esposito, S. Campopiano, and A. Iadicicco, "Mode transition phenomena into an in-fiber Mach-Zehnder interferometer," *Opt. Fiber Technol.*, vol. 80, Oct. 2023, Art. no. 103481, doi: [10.1016/j.yofte.2023.103481](https://doi.org/10.1016/j.yofte.2023.103481).
- [19] V. P. Zhdanov, "Basics of the LSPR sensors for soft matter at interfaces," *Plasmonics*, vol. 18, no. 3, pp. 971–982, Jun. 2023, doi: [10.1007/s11468-023-01812-1](https://doi.org/10.1007/s11468-023-01812-1).
- [20] V. Kumar, S. K. Raghuvanshi, and S. Kumar, "Recent advances in carbon nanomaterials based SPR sensor for biomolecules and gas detection—A review," *IEEE Sensors J.*, vol. 22, no. 16, pp. 15661–15672, Aug. 2022, doi: [10.1109/JSEN.2022.3191042](https://doi.org/10.1109/JSEN.2022.3191042).
- [21] Q. Wang et al., "Research advances on surface plasmon resonance biosensors," *Nanoscale*, vol. 14, no. 3, pp. 564–591, 2022, doi: [10.1039/D1NR05400G](https://doi.org/10.1039/D1NR05400G).
- [22] G. Li et al., "Graphene oxide/multiwalled carbon nanotubes assisted serial quadruple tapered structure-based LSPR sensor for glucose detection," *IEEE Sensors J.*, vol. 22, no. 17, pp. 16904–16911, Sep. 2022, doi: [10.1109/JSEN.2022.3193455](https://doi.org/10.1109/JSEN.2022.3193455).
- [23] B. K. Kaushik et al., "Detection of collagen-IV using highly reflective metal nanoparticles—Immobilized photosensitive optical fiber-based MZI structure," *IEEE Trans. Nanobiosci.*, vol. 19, no. 3, pp. 477–484, Jul. 2020, doi: [10.1109/TNB.2020.2998520](https://doi.org/10.1109/TNB.2020.2998520).
- [24] A. S. Sethulekshmi, J. S. Jayan, A. Saritha, and K. Joseph, "Insights into the reinforcing and multifarious role of WS₂ in polymer matrix," *J. Alloys Compounds*, vol. 876, Sep. 2021, Art. no. 160107, doi: [10.1016/j.jallcom.2021.160107](https://doi.org/10.1016/j.jallcom.2021.160107).
- [25] S.-W. Bai, H. Mei, W.-Z. Huang, M.-G. Zhang, and L.-F. Cheng, "In situ irradiated X-ray photoelectron spectroscopy on Ag-WS₂ heterostructure for hydrogen production enhancement," *J. Materomics*, vol. 7, no. 2, pp. 320–327, Mar. 2021, doi: [10.1016/j.jmat.2020.10.003](https://doi.org/10.1016/j.jmat.2020.10.003).
- [26] J. Z. Wu, S. A. Ghopry, B. Liu, and A. Shultz, "Metallic and non-metallic plasmonic nanostructures for LSPR sensors," *Micromachines*, vol. 14, no. 7, p. 1393, Jul. 2023, doi: [10.3390/mi14071393](https://doi.org/10.3390/mi14071393).
- [27] X. Chen et al., "Construction of plasmonic 1T-WS₂/2H-WS₂/CdS heterostructures for enhanced solar driven hydrogen evolution," *J. Mater. Chem. A*, vol. 10, no. 45, pp. 24030–24040, 2022, doi: [10.1039/D2TA07140A](https://doi.org/10.1039/D2TA07140A).
- [28] W. Lei et al., "Surface-structure sensitivity of CeO₂ nanocrystals in photocatalysis and enhancing the reactivity with nanogold," *ACS Catal.*, vol. 5, no. 7, pp. 4385–4393, Jul. 2015, doi: [10.1021/acscatal.5b00620](https://doi.org/10.1021/acscatal.5b00620).
- [29] S. Kumar, R. Singh, Q. Yang, S. Cheng, B. Zhang, and B. K. Kaushik, "Highly sensitive, selective and portable sensor probe using germanium-doped photosensitive optical fiber for ascorbic acid detection," *IEEE Sensors J.*, vol. 21, no. 1, pp. 62–70, Jan. 2021, doi: [10.1109/JSEN.2020.2973579](https://doi.org/10.1109/JSEN.2020.2973579).
- [30] B. D. Gupta and R. Kant, "Recent advances in surface plasmon resonance based fiber optic chemical and biosensors utilizing bulk and nanostructures," *Opt. Laser Technol.*, vol. 101, pp. 144–161, May 2018, doi: [10.1016/j.optlastec.2017.11.015](https://doi.org/10.1016/j.optlastec.2017.11.015).
- [31] V. P. Prakashan et al., "Novel SPR based fiber optic sensor for vitamin A using Au@Ag core-shell nanoparticles doped SiO₂-TiO₂-ZrO₂ ternary matrix," *Appl. Surf. Sci.*, vol. 484, pp. 219–227, Aug. 2019, doi: [10.1016/j.apsusc.2019.04.055](https://doi.org/10.1016/j.apsusc.2019.04.055).
- [32] H. Yockell-Lelièvre, F. Lussier, and J.-F. Masson, "Influence of the particle shape and density of self-assembled gold nanoparticle sensors on LSPR and SERS," *J. Phys. Chem. C*, vol. 119, no. 51, pp. 28577–28585, Dec. 2015, doi: [10.1021/acs.jpcc.5b09570](https://doi.org/10.1021/acs.jpcc.5b09570).
- [33] L. Singh, R. Singh, B. Zhang, B. K. Kaushik, and S. Kumar, "Localized surface plasmon resonance based hetero-core optical fiber sensor structure for the detection of L-cysteine," *IEEE Trans. Nanotechnol.*, vol. 19, pp. 201–208, 2020, doi: [10.1109/TNANO.2020.2975297](https://doi.org/10.1109/TNANO.2020.2975297).
- [34] Q. Lu et al., "A turn-on fluorescent probe for vitamin C based on the use of a silicon/CoOOH nanoparticle system," *Microchimica Acta*, vol. 186, no. 2, p. 72, Feb. 2019, doi: [10.1007/s00604-018-3181-z](https://doi.org/10.1007/s00604-018-3181-z).
- [35] I. Š. Rončević, D. Skroza, I. Vrca, A. M. Kondža, and N. Vladislavić, "Development and optimization of electrochemical method for determination of vitamin C," *Chemosensors*, vol. 10, no. 7, p. 283, Jul. 2022, doi: [10.3390/chemosensors10070283](https://doi.org/10.3390/chemosensors10070283).
- [36] A. Hatefi-Mehrjardi, M. A. Karimi, M. Soleymanzadeh, and A. Barani, "Highly sensitive detection of dopamine, ascorbic and uric acid with a nanostructure of dianix yellow/multi-walled carbon nanotubes modified electrode," *Measurement*, vol. 163, Oct. 2020, Art. no. 107893, doi: [10.1016/j.measurement.2020.107893](https://doi.org/10.1016/j.measurement.2020.107893).
- [37] S. Wen, M. Huang, R. Cheng, J. Gao, and J. Wang, "Silver-coated gold nanorods as optical probes for the sensitive detection of ascorbic acid in tablets," *Chemosensors*, vol. 10, no. 12, p. 543, Dec. 2022, doi: [10.3390/chemosensors10120543](https://doi.org/10.3390/chemosensors10120543).
- [38] N. V. Saranchina et al., "Rapid colorimetric determination of ascorbic acid by solid phase extraction of iodine into a polymethacrylate matrix," *Mendeleev Commun.*, vol. 32, no. 1, pp. 136–138, Jan. 2022, doi: [10.1016/j.mencom.2022.01.044](https://doi.org/10.1016/j.mencom.2022.01.044).
- [39] B. Ibarlucea, A. P. Roig, D. Belyaev, L. Baraban, and G. Cuniberti, "Electrochemical detection of ascorbic acid in artificial sweat using a flexible alginate/CuO-modified electrode," *Microchimica Acta*, vol. 187, no. 9, p. 520, Aug. 2020, doi: [10.1007/s00604-020-04510-5](https://doi.org/10.1007/s00604-020-04510-5).